Bull. Aust. Math. Soc. **100** (2019), 109–118
doi:10.1017/S0004972719000297

SYMMETRIC ITINERARY SETS: ALGORITHMS AND NONLINEAR EXAMPLES

BRENDAN HARDING

(Received 10 December 2018; accepted 2 February 2019; first published online 20 March 2019)

Abstract

We describe how to approximate fractal transformations generated by a one-parameter family of dynamical systems $W : [0,1] \to [0,1]$ constructed from a pair of monotone increasing diffeomorphisms W_i such that $W_i^{-1} : [0,1] \to [0,1]$ for $i = 0, 1$. An algorithm is provided for determining the unique parameter value such that the closure of the symbolic attractor $\overline{\Omega}$ is symmetrical. Several examples are given, one in which the W_i are affine and two in which the W_i are nonlinear. Applications to digital imaging are also discussed.

2010 *Mathematics subject classification*: primary 37E05; secondary 28A80, 94A08.

Keywords and phrases: expanding dynamical system, fractal transformation, chaos game algorithm.

1. Introduction

This article describes algorithms for the construction of fractal transformations from a one parameter family of dynamical systems $W : [0,1] \to [0,1]$ as described in [3]. Of particular interest is the specific case in which the underlying itinerary set is symmetric (which occurs for exactly one value of the parameter ρ which parametrises W) and several examples are provided. Applications to digital imaging, similar to those described in [2] for the special case of affine dynamical systems, are also briefly discussed.

For completeness we recall the basic setup from [3]. Let $W_0 : [0,a] \to [0,1]$ and $W_1 : [1-b,1] \to [0,1]$ be continuous and differentiable and such that $a + b > 1$, $W_0(0) = W_1(1-b) = 0$, $W_0(a) = W_1(1) = 1$. Let the derivatives $W_i'(x)$ $(i = 0, 1)$ be uniformly bounded below by $d > 1$. For $\rho \in [1-b, a]$ we define $W : [0,1] \to [0,1]$ by

$$[0,1] \ni x \mapsto \begin{cases} W_0(x) & \text{if } x \in [0,\rho], \\ W_1(x) & \text{otherwise.} \end{cases}$$

Similarly, we define $W_+ : [0,1] \to [0,1]$ by replacing $[0,\rho]$ by $[0,\rho)$.

The author acknowledges support from an Australian Research Council Discovery Project (project number DP160102021) funded by the Australian Government.

Let $I = \{0, 1\}$. Let $I^\infty = \{0, 1\} \times \{0, 1\} \times \cdots$ have the product topology induced from the discrete topology on I. For $\sigma \in I^\infty$ write $\sigma = \sigma_0\sigma_1\sigma_2 \cdots$, where $\sigma_k \in I$ for all $k \in \mathbb{N}$. The product topology on I^∞ is the same as the topology induced by the metric $d(\omega, \sigma) = 2^{-k}$ where k is the least index such that $\omega_k \neq \sigma_k$. It is well known that (I^∞, d) is a compact metric space. We define a total order relation $\preceq$ on I^∞, and on I^n for any $n \in \mathbb{N}$, by $\sigma \prec \omega$ if $\sigma \neq \omega$ and $\sigma_k < \omega_k$ where k is the least index such that $\sigma_k \neq \omega_k$. For $\sigma \in I^\infty$ and $n \in \mathbb{N}$ we write $\sigma|_n = \sigma_0\sigma_1\sigma_2 \cdots \sigma_n$. Given $n \in \mathbb{N}$ and $\kappa \in I^n$, denote by $\bar{\kappa}$ the periodic address $\kappa\kappa\kappa \cdots \in I^\infty$. We define a symmetry function $^* : I^\infty \to I^\infty$ by $\sigma^* = \omega$ where $\omega_k = 1 - \sigma_k$ for all k. By slight abuse of notation, we may also denote this as $\sigma^* = \bar{1} - \sigma$ where the subtraction is performed elementwise over the symbols. Let $S : I^\infty \to I^\infty$ denote the left shift map $\sigma_0\sigma_1\sigma_2 \cdots \mapsto \sigma_1\sigma_2 \cdots$ for all $\sigma \in I^\infty$.

For $k \in \mathbb{N}$, let $W^k = W \circ \cdots \circ W$ (k times) and $W_+^k = W_+ \circ \cdots \circ W_+$ (k times). We define a map $\tau : [0, 1] \to I^\infty$, using all of the orbits of W, by

$$\tau(x) = \sigma_0\sigma_1\sigma_2 \cdots$$

where σ_k equals 0 or 1, according as $W^k(x) \in [0, \rho]$ or $(\rho, 1]$, respectively. We call $\tau(x)$ the *itinerary* of x under W, or an *address* of x, and we call $\Omega = \tau([0, 1])$ an *address space* for $[0, 1]$. Similarly, we define $\tau^+ : [0, 1] \to I^\infty$ so that $\tau^+(x)_k$ equals 0 or 1, according as $W_+^k(x) \in [0, \rho)$ or $[\rho, 1]$, respectively; and we define $\Omega_+ = \tau^+([0, 1])$. Let $\overline{\Omega}$ denote the closure of Ω. Note that W, W_+, Ω, Ω_+, $\overline{\Omega}$, τ, and τ^+ all depend on ρ.

Recall that the projection $\hat{\pi} : I^\infty \to [0, 1]$ is well-defined by

$$\hat{\pi}(\sigma) = \sup\{x \in [0, 1] : \tau^+(x) \preceq \sigma\} = \inf\{x \in [0, 1] : \tau(x) \succeq \sigma\}.$$

Furthermore, $\hat{\pi}$ is increasing and continuous and

$$\hat{\pi}(\tau(x)) = \hat{\pi}(\tau^+(x)) = x \quad \text{for all } x \in [0, 1],$$
$$\tau(\hat{\pi}(\sigma)) \preceq \sigma \preceq \tau^+(\hat{\pi}(\sigma)) \quad \text{for all } \sigma \in I^\infty.$$

Additionally, it is a standard result that

$$\hat{\pi}(\sigma) = \lim_{k\to\infty} W_{\sigma_0}^{-1} \circ W_{\sigma_1}^{-1} \circ \cdots \circ W_{\sigma_k}^{-1}(y),$$

noting that the limit exists and is uniquely defined for any $y \in [0, 1]$ (because $W_0^{-1}, W_1^{-1} : [0, 1] \to [0, 1]$ are contractions with contractivity factor at most d^{-1}). This is particularly useful for computing the projection of a given σ. Given a truncated address $\sigma|_n$ we take $\hat{\pi}$ to map $\sigma|_n$ to the interval

$$\hat{\pi}(\sigma|_n) = [W_{\sigma_0}^{-1} \circ W_{\sigma_1}^{-1} \circ \cdots \circ W_{\sigma_n}^{-1}(0), W_{\sigma_0}^{-1} \circ W_{\sigma_1}^{-1} \circ \cdots \circ W_{\sigma_n}^{-1}(1)]$$

which has length at most d^{-n}. It follows that the approximation of $\hat{\pi}(\sigma)$ by either end point has error bounded above by d^{-n}.

We also repeat a few results which are relevant to this work.

Lemma 1.1 [3, Lemma 4.1]. *For all $\rho \in [1 - b, a]$,*

$$\overline{\Omega} = \{\sigma \in I^\infty : \textit{for all } k \in \mathbb{N},\ \sigma_k = 0 \Rightarrow S^k(\sigma) \preceq \tau(\rho) \textit{ and } \sigma_k = 1 \Rightarrow \tau^+(\rho) \preceq S^k(\sigma)\}.$$

https://doi.org/10.1017/S0004972719000297 Published online by Cambridge University Press

Corollary 1.2 [3, Corollary 4.2]. *$\overline{\Omega}$ is symmetric if and only if $\tau(\rho) = (\tau^+(\rho))^*$.*

Lemma 1.3 [3, Lemma 4.3]. *The maps $\tau(\rho)$ and $\tau^+(\rho)$ are strictly increasing as functions of $\rho \in [1-b, a]$ to I^∞.*

Theorem 1.4 [3, Theorem 1.2]. *There exists a unique $\rho \in [1-b, a]$ such that $\overline{\Omega}^* = \overline{\Omega}$.*

2. The determination of ρ such that $\overline{\Omega}$ is symmetric

We introduce an extended address space by $J^\infty = J \times J \times \cdots$ which has the product topology induced from the discrete topology on $J = \{-1, 0, 1\}$. For $\sigma \in J^\infty$ we write $\sigma = \sigma_0\sigma_1\sigma_2\cdots$ where $\sigma_k \in J$ for all $k \in \mathbb{N}$. We define a signed distance function (common in the context of level set methods and implicit surfaces, see for example [8]) over J^∞, and on J^n, by $d_s(\sigma, \omega) = (\omega_k - \sigma_k)3^{-k}$ where k is the least index such that $\omega_k \neq \sigma_k$. Notice that $|d_s(\sigma, \omega)|$ is a metric on J^∞ that induces a topology equivalent to the product topology. We define a total order relation $\preceq$ on J^∞, and on J^n for any $n \in \mathbb{N}$, by $\sigma \prec \omega$ if $\sigma \neq \omega$ and $\sigma_k < \omega_k$ where k is the least index such that $\sigma_k \neq \omega_k$. Notice that $\sigma \prec \omega$ if and only if $d_s(\sigma, \omega) > 0$.

Consider the mapping $\Gamma : [1-b, a] \to J^\infty$ defined by

$$\Gamma(\rho) = \tau^+(\rho) - \tau(\rho)^*,$$

where the subtraction is taken elementwise over the addresses, that is

$$\Gamma(\rho)_k = \tau^+(\rho)_k - (1 - \tau(\rho)_k).$$

Equivalently, by slight abuse of notation, we may write $\Gamma(\rho) = \tau^+(\rho) + \tau(\rho) - \bar{1}$.

Lemma 2.1. *$\overline{\Omega}$ is symmetric if and only if $\Gamma(\rho) = \bar{0}$. Furthermore, $\Gamma(\rho)$ is a strictly increasing function of $\rho \in [1-b, a]$ to J^∞.*

Proof. The first claim is essentially identical to Corollary 1.2. Since τ^+ and τ are strictly increasing (Lemma 1.3) it follows immediately that Γ is strictly increasing. □

Corollary 2.2. *$\overline{\Omega}$ is symmetric if and only if $d_s(\tau(\rho)^*, \tau^+(\rho)) = 0$. Furthermore, $\rho \mapsto d_s(\tau(\rho)^*, \tau^+(\rho))$ is a nondecreasing function of $\rho \in [1-b, a]$ into $\mathbb{R}$.*

This follows immediately by noticing that $d_s(\bar{0}, \tau^+(\rho) - \tau(\rho)^*) = d_s(\tau(\rho)^*, \tau^+(\rho))$ and that $\sigma \preceq \omega$ implies $d_s(\bar{0}, \sigma) \leq d_s(\bar{0}, \omega)$. The mapping $\rho \mapsto d_s(\tau(\rho)^*, \tau^+(\rho))$ is nondecreasing (rather than strictly increasing) because only the first index k for which the addresses differ is taken into account. As an aside, note that we could alternatively introduce a signed distance function

$$d'_s(\sigma, \omega) = \sum_{k=0}^{\infty} (\omega_k - \sigma_k)a^k$$

for any $a \in (0, 1/2)$ (observe one cannot take $a = 1/2$ or else one would have $d'_s(0\bar{1}, 1\bar{0}) = 0$). The mapping $\rho \mapsto d'_s(\tau(\rho)^*, \tau^+(\rho))$ is then strictly increasing.

https://doi.org/10.1017/S0004972719000297 Published online by Cambridge University Press

Algorithm 1 Bisection algorithm for determining the ρ such that $\overline{\Omega}$ is symmetric.

In. Functions τ, τ^+ and $a, b \in [0,1]$ corresponding to a dynamical system W.
0. Set $\rho_L = 1 - b$, $\rho_R = a$.
1. Set $\rho_C = (\rho_L + \rho_R)/2$.
2. If $d_s(\tau(\rho_L)^*, \tau^+(\rho_L)) \times d_s(\tau(\rho_C)^*, \tau^+(\rho_C)) \leq 0$ set $\rho_R = \rho_C$, otherwise set $\rho_L = \rho_C$.
3. Repeat from 1 until $\rho_R - \rho_L$ and/or $d_s(\tau(\rho_C)^*, \tau^+(\rho_C))$ are less than some desired tolerance(s).

Out. $\rho_C = (\rho_L + \rho_R)/2$.

These results, along with Theorem 1.4, are useful as they guarantee that the bisection method can be used to determine the unique ρ such that $\overline{\Omega}$ is symmetric. Specifically one may determine ρ via Algorithm 1. In practice the calculation of $\tau(\rho_L), \tau^+(\rho_L), \tau(\rho_C), \tau^+(\rho_C)$ in step 2 is done up to some finite address length n and the signed distances are estimated using the truncated address. If it is desired that the bisection method terminate when $\rho_R - \rho_L < \epsilon$ for some $\epsilon > 0$ then n should be large enough that $(a + b - 1)d^{-n} < \epsilon$. Note that $d_s(\tau(\rho)^*, \tau^+(\rho))$ is neither continuous nor differentiable and thus one cannot use methods which require continuity and/or smoothness to perform well (such as Newton's method). The alternative signed distance function d_s' could be used in the algorithm but offers no advantage except at the end where one can definitively determine which of ρ_L, ρ_C, ρ_R is closer to the desired ρ.

3. The approximation of $h(x)$

We now take a moment to describe how one may approximate a fractal transformation $h : [0,1] \to [0,1]$ defined as

$$h(x) := 1 - \hat{\pi}(\tau(x)^*).$$

Note this definition differs slightly from that in [3] so that h is increasing (with $h(0) = 0$ and $h(1) = 1$) rather than decreasing. Of particular interest is the case when ρ is the unique value in $[1 - b, a]$ such that $\overline{\Omega}$ is symmetric in which case h is a homeomorphism (although the algorithms described below work for any $\rho \in [1 - b, a]$ but will otherwise result in an h which is discontinuous as in Example 4.2). A direct approach is to choose a (finite) integer $n > 0$ and then simply approximate $h(x)$ as an element of the interval $1 - \hat{\pi}((\tau(x)|_n)^*)$. A reasonable approximation is

$$h(x) \approx 1 - W^{-1}_{1-\tau(x)_0} \circ W^{-1}_{1-\tau(x)_1} \circ \cdots \circ W^{-1}_{1-\tau(x)_n}(1/2)$$

which, in the case of affine maps, is in the centre of the interval and thus has error at most $\frac{1}{2}d^{-n}$ (assuming the computation of $\tau(x)|_n$ is exact). By computing $h(x)$ for equidistant samples $x \in [0,1]$, one can approximate the graph of $h(x)$ in the usual way.

https://doi.org/10.1017/S0004972719000297 Published online by Cambridge University Press

Note that for increasing n it becomes more likely that there are errors in the latter digits of $\tau(x)|_n$ because W is an expanding map and thus floating point rounding errors grow geometrically. For instance, with double precision arithmetic it is unlikely that the trailing elements of addresses longer than the smallest n such that $d^n > 2^{53}$ will be accurate.

Algorithm 2 Chaos game algorithm for approximating the mapping $x \mapsto h(x)$.

In. Integers $N, M, K > 0$ and the addresses $\tau(\rho)|_n, \tau^+(\rho)|_n$.
0. Set $\sigma_n = 0$ for $n = 0, \dots, N$, and $H_m = Q_m = 0$ for $m = 0, \dots, M$, and $k = q = x = y = 0$.
1. Randomly choose $r \in \{0, 1\}$, set $\sigma_{n+1} = \sigma_n$ for $n = 0, \dots, N-1$ and then $\sigma_0 = r$.
2. If $r = 0$ then set $x = W_0^{-1}(x)$ and $y = 1 - W_1^{-1}(1-y)$, else (i.e. $r = 1$) set $x = W_1^{-1}(x)$ and $y = 1 - W_0^{-1}(1-y)$.
3. If $r = 0$ and $d_s(\sigma|_n, \tau(\rho)|_n) < 0$, then set $q = 0$, else if $r = 1$ and $d_s(\tau^+(\rho)|_n, \sigma|_n) < 0$, then set $q = 0$.
4. Set $k = \text{Round}(xM)$, if $Q_k < q$ then set $Q_k = q$ and $H_k = y$.
5. Set $q = q + 1$ and $k = k + 1$, if $k < K$ repeat from step 1.

Out. Array H which can be plotted against $X = \{m/M\}_{m=0,\dots,M}$ to approximate $h(x)$.

An alternative method for approximating the graph of $h(x)$ is based on a modification of the classical chaos game algorithm [1]. This is guaranteed to be stable because only contractive maps are used. A basic outline is described in Algorithm 2. The input integers N, M, K determine the length of the truncated address which is recorded, the number of sub-intervals (each with equal length) that the interval $[0, 1]$ is divided into and the total number of iterations respectively. Observe that the purpose of q, Q is to measure the quality of the best current approximation of h. Recall from Lemma 1.1 that $\omega \in \overline{\Omega}$ if and only if for all $k \in \mathbb{N}$, $\sigma_k = 0$ implies $S^k(\sigma) \preceq \tau(\rho)$ and $\sigma_k = 1$ implies $S^k(\sigma) \succeq \tau^+(\rho)$. Therefore q tracks the number of successive iterations for which the truncated address $\sigma|_n$ generated by the chaos game is a valid member of the truncated address space $\overline{\Omega}|_n = \{\omega|_n : \omega \in \overline{\Omega}\}$. As q increases the iterations become better converged. An alternative stopping criterion (to the fixed number of iterates K) is to stop when the minimum of the array Q is equal to some $q_{\min}$ (which generally should be at most N). Note that there is an implicit assumption here that the $\tau(\rho)|_n, \tau^+(\rho)|_n$ are exact. In the case that ρ is such that $\overline{\Omega}$ is symmetric then only $\tau(\rho)|_n$ need be provided as $\tau^+(\rho)|_n = (\tau(\rho)|_n)^*$.

We take a moment to illustrate why y in Algorithm 2 gives an approximation of $h(x)$. Let us define the dynamical system

$$W^*(x) = \begin{cases} 1 - W_1(1-x) & \text{if } x \in [0, 1-\rho), \\ 1 - W_0(1-x) & \text{otherwise,} \end{cases}$$

and the corresponding address function $\tau^* : [0, 1] \to I^\infty$ where $\tau^*(x)_k$ is 0 if $(W^*)^k(x)$

https://doi.org/10.1017/S0004972719000297 Published online by Cambridge University Press

is in $[0, 1-\rho)$ and is 1 otherwise. Introduce the projection $\hat{\pi}^*$ for which $\hat{\pi}^*(\tau^*(x)) = x$ for all $x \in [0,1]$ and define the mapping $h^* : [0,1] \to [0,1]$ by $h^*(x) = 1 - \hat{\pi}^*(\tau^*(x)^*)$.

LEMMA 3.1. *$\hat{\pi}^*(\tau(x)) = h(x)$ and $h(x) = 1 - h^*(1-x)$.*

PROOF. It is straightforward to show that $\tau(x)^* = \tau^*(1-x)$ and $\hat{\pi}(\sigma^*) = 1 - \hat{\pi}^*(\sigma)$. Consequently,

$$\hat{\pi}^*(\tau(x)) = 1 - \hat{\pi}(\tau(x)^*) = h(x)$$

and

$$h(x) = 1 - \hat{\pi}(\tau(x)^*) = \hat{\pi}^*(\tau^*(1-x)^*) = 1 - h^*(1-x),$$

as required. □

It follows from this lemma that the iteration of $(W^*)^{-1}$ on y in step 2 is such that $y \to h(x)$ as q increases.

The basic algorithm outlined above can be further modified to improve efficiency in the sense of having the smallest number of iterations such that every $\sigma_0\sigma_1\cdots\sigma_n \in I^{n+1}$ appears at least once. In particular, rather than randomly choosing $r \in \{0,1\}$ over some desired K iterations one can instead iterate over a deBruijn sequence (an approach explored for approximating attractors of iterated function systems in [4–6]). For instance, a deBruijn sequence with base 2 and order $n+1$ is a sequence with the shortest possible length (2^{n+1}) such that every $\sigma_0\sigma_1\cdots\sigma_n \in I^{n+1}$ appears exactly once (noting one needs to wrap around the ends to get the last n sub-sequences). In contrast, iterating $K = 2^{n+1}$ times with a pseudorandom number generator has vanishingly small probability of generating every $\sigma_0\sigma_1\cdots\sigma_n \in I^{n+1}$. Additionally, the smallest such deBruijn sequence (with respect to the ordering $\prec$ on $I^{2^{n+1}}$) can be generated in constant amortised time [7] and is in practice comparable (if not faster) than producing 2^{n+1} random numbers with a high quality pseudorandom number generator.

4. Examples and applications to digital imaging

We first provide an example based on affine maps. The existence and uniqueness of a ρ that gives rise to a fractal homeomorphism in the special case of affine maps was first described in [2] and additional examples can be found there.

EXAMPLE 4.1. Let W_a, depicted in Figure 1(a), denote the dynamical system arising from the affine maps

$$W_0(x) = \tfrac{3}{2}x, \qquad W_1(x) = \tfrac{5}{3}x - \tfrac{2}{3}.$$

Here, W_a is parametrised by $\rho \in [2/5, 2/3]$. The symbolic attractor $\overline{\Omega}$ is symmetric for $\rho \approx 0.554383369$. The corresponding homeomorphism, denoted by $h_a(x)$, is plotted in Figure 1(b). The function $h_a(x) - x$ is also plotted in Figure 1(c) to better illustrate how the homeomorphism differs from the identity map.

In the next example, the dynamical system consists of quadratic maps.

https://doi.org/10.1017/S0004972719000297 Published online by Cambridge University Press

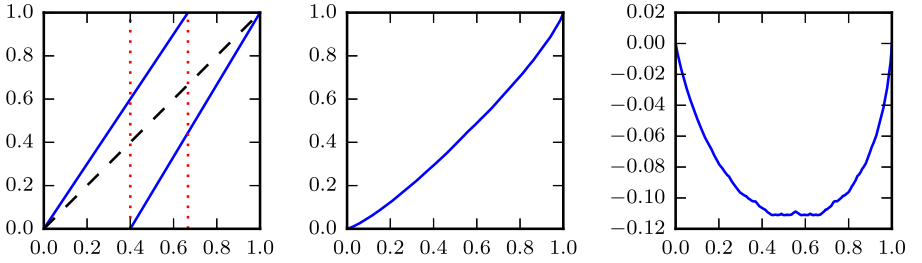

(a) plot of W_a (b) plot of $y = h_a(x)$ (c) plot of $y = h_a(x) - x$

FIGURE 1. Example of a dynamical system and the corresponding homeomorphism constructed from affine maps as in Example 4.1 (colour available online).

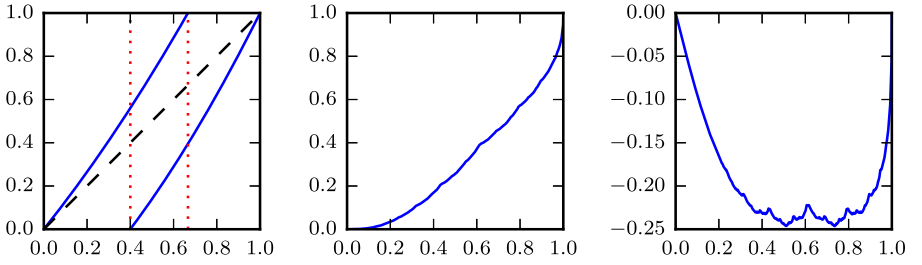

(a) plot of W_q (b) plot of $y = h_q(x)$ (c) plot of $y = h_q(x) - x$

FIGURE 2. Example of a dynamical system and the corresponding homeomorphism constructed from quadratic maps as in Example 4.2 (colour available online).

EXAMPLE 4.2. Let W_q, depicted in Figure 2(a), denote the dynamical system arising from the quadratic maps

$$W_0(x) = \tfrac{5}{4}x + \tfrac{3}{8}x^2, \quad W_1(x) = -\tfrac{4}{9} + \tfrac{8}{9}x + \tfrac{5}{9}x^2.$$

Here, W_q is parametrised by $\rho \in [2/5, 2/3]$. The symbolic attractor $\overline{\Omega}$ is symmetric for $\rho \approx 0.611327690$. The corresponding homeomorphism, denoted by $h_q(x)$, is plotted in Figure 2(b). The function $h_q(x) - x$ is also plotted in Figure 2(c) to better illustrate how the homeomorphism differs from the identity map. In Figure 3 we also provide an example of the mappings obtained if ρ is taken as $1 - b = 2/5$ in (a) and $a = 2/3$ in (b). These two extremes demonstrate typical properties of fractal transformations generated via a code space which is nonsymmetric.

Observe that the quadratic maps of Example 4.2 were chosen so that the domain of ρ is the same as that in Example 4.1. Despite the W_i having the same endpoints in each case (within $[0, 1]^2$) it is clear that the features of the homeomorphism are more extreme in the case of the quadratic maps.

https://doi.org/10.1017/S0004972719000297 Published online by Cambridge University Press

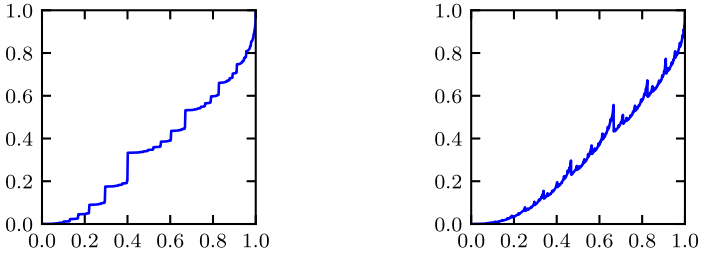

(a) plot of h obtained from W_q with $\rho = 2/5$ (b) plot of h obtained from W_q with $\rho = 2/3$

FIGURE 3. Example of the mappings h generated from W_q when ρ differs from the value for which $\overline{\Omega}$ is symmetric as in Example 4.2 (colour available online).

We now describe an additional example in which the dynamical system consists of nonlinear mappings.

EXAMPLE 4.3. Let W_n, depicted in Figure 4(a), denote the dynamical system arising from the nonlinear maps

$$W_0(x) = \frac{3}{2}x + \frac{1}{15\pi}\sin(6\pi x),$$
$$W_1(x) = -\frac{1}{2} - \frac{2}{9\pi} + \left(\frac{3}{2} + \frac{1}{3\pi}\right)x - \frac{1}{9\pi}\cos\left(\frac{9\pi}{2}(1-x)\right).$$

Here, W_n is parametrised by $\rho \in [1/3, 2/3]$. The symbolic attractor $\overline{\Omega}$ is symmetric for $\rho \approx 0.513711977$. The corresponding homeomorphism, denoted by $h_n(x)$, is plotted in Figure 4(b). The function $h_n(x) - x$ is also plotted in Figure 4(c) to better illustrate how the homeomorphism differs from the identity map.

In the above example the sign of each W_i'' changes multiple times. Notice how, unlike the previous two examples, there are solutions to $h_n(x) = x$ on the interior of $[0, 1]$.

We now consider the application to digital imaging. In notation similar to that of [2], let $\mathcal{B}$ be a *picture* function of the form

$$\mathcal{B} : [0,1]^2 \to C$$

where C is a colour space (for instance $\{0, 1, \ldots, 255\}^3$ for a standard RGB bitmap image). Here we take $\mathcal{B}$ to also encapsulate the discretisation of the unit square to the resolution of a given picture. Let $h, \tilde{h} : [0, 1] \to [0, 1]$ denote homeomorphisms constructed from the symmetric itinerary set of some given dynamical systems $W, \tilde{W}$. These homeomorphisms may be applied along the x, y coordinates of an image respectively via the composition

$$(\mathcal{B} \circ (h \otimes \tilde{h}))(x, y) = \mathcal{B}(h(x), \tilde{h}(y)).$$

In this way the transformations can be used for image beautification, roughening, and special effects.

https://doi.org/10.1017/S0004972719000297 Published online by Cambridge University Press

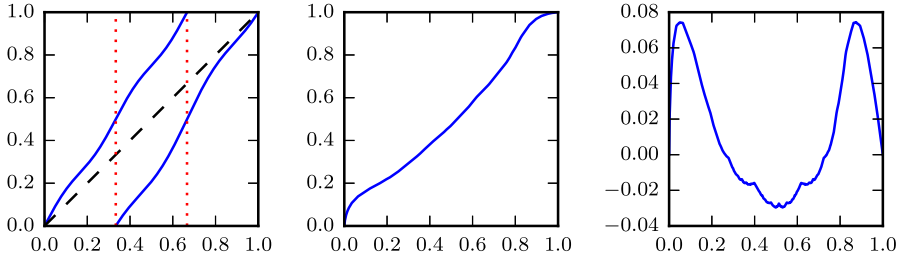

(a) plot of W_n (b) plot of $y = h_n(x)$ (c) plot of $y = h_n(x) - x$

FIGURE 4. Example of a dynamical system and the corresponding homeomorphism constructed from nonlinear maps as in Example 4.3 (colour available online).

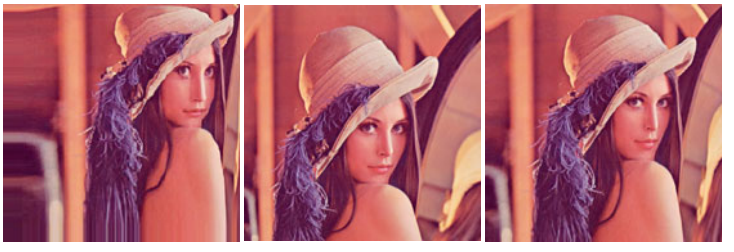

(a) non-linear maps (b) original (c) affine maps

FIGURE 5. Fractal homeomorphisms applied to the Lena test image. Refer to Example 4.4 for details. Note that the origin is taken to be the bottom left corner unlike the usual convention in imaging sciences. (Colour available online.)

EXAMPLE 4.4. Two examples of $\mathcal{B} \circ (h \otimes \tilde{h})$ (with $\tilde{h} = h$ in each case) are shown in Figure 5. Specifically, Figure 5(b) shows $\mathcal{B}$ applied to the unit square whereas Figures 5(a,c) show the result of $\mathcal{B} \circ (h_q \otimes h_q)$ and $\mathcal{B} \circ (h_a \otimes h_a)$ respectively.

The homeomorphisms can also be used for image filtering analogous to that described in [2]. Specifically, if $\mathcal{D} : [0,1]^2 \to [0,1]^2$ denotes the digitisation operation that discretises the unit square to the resolution of the image onto which $\mathcal{B}$ maps (and as such $\mathcal{B} \circ \mathcal{D} = \mathcal{B}$), then an image filter can be constructed from $h, \tilde{h}$ as

$$(h^{-1} \otimes \tilde{h}^{-1}) \circ \mathcal{D} \circ (h \otimes \tilde{h}).$$

The effect of such filters is often subtle and difficult to visually distinguish from the original image.

EXAMPLE 4.5. An example of a fractal filter applied to the peppers test image is shown in Figure 6. Specifically, in this example we take $h = h_n$ and $\tilde{h} = h_q$. Figure 6(a) shows the original image, Figure 6(b) shows the transformation of the image via $\mathcal{B} \circ (h_n \otimes h_q)$ and Figure 6(c) shows the effect of the filter $(h_n^{-1} \otimes h_q^{-1}) \circ \mathcal{D} \circ (h_n \otimes h_q)$. Notice the filter is most extreme in the vertical direction near the top and bottom owing

https://doi.org/10.1017/S0004972719000297 Published online by Cambridge University Press

(a) original image (b) transformed image (c) filtered image

FIGURE 6. Fractal filter applied to the peppers test image. Refer to Example 4.5 for details. Note that the origin is taken to be the bottom left corner unlike the usual convention in imaging sciences. (Colour available online.)

to the extreme compression and stretching caused by h_q in these regions respectively, whereas the horizontal effect from h_n is much more subtle.

We also refer the reader to the example using affine dynamical systems in [2].

References

[1] M. F. Barnsley, *Fractals Everywhere*, 2nd edn (Academic Press, London, 1993).
[2] M. F. Barnsley, B. Harding and K. Igudesman, 'How to transform and filter images using iterated function systems', *SIAM J. Imaging Sci.* **4**(4) (2011), 1001–1028.
[3] M. F. Barnsley and N. Mihalache, 'Symmetric itinerary sets', *Bull. Aust. Math. Soc.*, to appear.
[4] S. G. Hoggar and I. Mcfarlane, 'Faster fractal pictures by finite fields and far rings', *Discrete Math.* **138**(1) (1995), 267–280.
[5] I. McFarlane and S. G. Hoggar, 'Optimal drivers for the 'random' iteration algorithm', *Comput. J.* **37**(7) (1994), 629–640.
[6] F. Mendivil, 'Fractals, graphs, and fields', *Amer. Math. Monthly* **110**(6) (2003), 503–515.
[7] F. Ruskey, C. Savage and T. M. Y. Wang, 'Generating necklaces', *J. Algorithms* **13**(3) (1992), 414–430.
[8] S. Osher and R. Fedkiw, 'Signed distance functions', in: *Level Set Methods and Dynamic Implicit Surfaces* (eds. S. Osher and R. Fedkiw) (Springer, New York, 2003), 17–22.

BRENDAN HARDING, School of Mathematical Sciences,
The University of Adelaide, Adelaide, South Australia 5005, Australia
e-mail: brendan.harding@adelaide.edu.au

https://doi.org/10.1017/S0004972719000297 Published online by Cambridge University Press